Effects of Proximal Tubule Shortening on Protein Excretion in a Lowe Syndrome Model

Megan L. Gliozzi,[1] Eugenel B. Espiritu,[2] Katherine E. Shipman,[1] Youssef Rbaibi,[1] Kimberly R. Long,[1] Nairita Roy,[3] Andrew W. Duncan,[3] Matthew J. Lazzara,[4] Neil A. Hukriede,[2,5] Catherine J. Baty,[1] and Ora A. Weisz[1]

[1]Renal-Electrolyte Division, Department of Medicine, [2]Department of Developmental Biology, and [3]Department of Pathology, McGowan Institute for Regenerative Medicine, and Pittsburgh Liver Research Center, Pittsburgh, Pennsylvania; [4]Department of Chemical Engineering, University of Virginia, Charlottesville, Virginia; and [5]Center for Critical Care Nephrology, University of Pittsburgh School of Medicine, Pittsburgh, Pennsylvania

ABSTRACT

Background Lowe syndrome (LS) is an X-linked recessive disorder caused by mutations in *OCRL*, which encodes the enzyme OCRL. Symptoms of LS include proximal tubule (PT) dysfunction typically characterized by low molecular weight proteinuria, renal tubular acidosis (RTA), aminoaciduria, and hypercalciuria. How mutant *OCRL* causes these symptoms isn't clear.

Methods We examined the effect of deleting OCRL on endocytic traffic and cell division in newly created human PT CRISPR/Cas9 *OCRL* knockout cells, multiple PT cell lines treated with *OCRL*-targeting siRNA, and in *orcl*-mutant zebrafish.

Results OCRL-depleted human cells proliferated more slowly and about 10% of them were multinucleated compared with fewer than 2% of matched control cells. Heterologous expression of wild-type, but not phosphatase-deficient, OCRL prevented the accumulation of multinucleated cells after acute knockdown of OCRL but could not rescue the phenotype in stably edited knockout cell lines. Mathematic modeling confirmed that reduced PT length can account for the urinary excretion profile in LS. Both *ocrl* mutant zebrafish and zebrafish injected with *ocrl* morpholino showed truncated expression of megalin along the pronephric kidney, consistent with a shortened S1 segment.

Conclusions Our data suggest a unifying model to explain how loss of OCRL results in tubular proteinuria as well as the other commonly observed renal manifestations of LS. We hypothesize that defective cell division during kidney development and/or repair compromises PT length and impairs kidney function in LS patients.

JASN 31: 67–83, 2020. doi: https://doi.org/10.1681/ASN.2019020125

The X-linked disease Lowe syndrome (LS) is caused by mutations in the gene *OCRL* that encodes the phosphatidylinositol 5′-phosphatase OCRL. Individuals with LS exhibit congenital cataracts, hypotonia, intellectual disability, and renal proximal tubule (PT) dysfunction. Low molecular weight (LMW) proteinuria is observed within the first few months after birth, and renal tubular acidosis (RTA), hypercalciuria, and aminoaciduria are also commonly observed.[1] Although their renal dysfunction has commonly been classified as Fanconi syndrome, glycosuria is strikingly absent in patients with LS.[2] Most patients with LS ultimately develop ESRD, often within the first 20 years of life.[1]

Understanding how the loss of OCRL impairs PT function has been challenging. Because phosphatidylinositol 4,5-bisphosphate [PtdIns(4,5)P2], the

Received February 8, 2019. Accepted September 24, 2019.

E.E. and K.E.S. contributed equally to this work.

Published online ahead of print. Publication date available at www.jasn.org.

Correspondence: Dr. Ora A. Weisz, Renal Electrolyte Division, University of Pittsburgh Medicine, 978.1 Scaife Hall, 3550 Terrace Street, Pittsburgh, PA 15261. Email: weisz@pitt.edu

Copyright © 2020 by the American Society of Nephrology

substrate of OCRL, is a major regulator of endocytosis, it has been anticipated that LMW proteinuria in patients with LS is due to some deficient function along the PT apical endocytic pathway.[3] Consistent with this, a subset of studies in cultured cell models demonstrate that OCRL plays a role in endocytic recycling, specifically by preventing the depolymerization of actin coats that accumulate on endocytic vesicles and/or recycling compartments.[4,5] However, OCRL also has many other roles in cell homeostasis, including ciliary biogenesis,[6–8] cell polarity, and autophagy.[6,9,10] Moreover, OCRL is recruited to the site of abscission during cytokinesis.[11] PtdIns(4,5)P_2 accumulation stabilizes the intracellular bridge during cytokinesis, and its hydrolysis by OCRL is necessary for abscission.[11] It remains unclear how impairment of these functions contributes to LS pathology. Another unanswered question is how loss of OCRL impairs PT recovery of Ca^{2+}, HCO_3^-, and amino acids in patients with LS.

Mouse and zebrafish models for LS have been developed in recent years, but a link between the molecular and cellular defects observed in cell culture and the phenotype of patients and animal models remains elusive. Transgenic zebrafish lacking OCRL exhibit reduced levels of megalin, reduced uptake of a fluid phase marker, and fewer subapical vesicles in the pronephric kidney PT, in addition to eye and facial defects consistent with those observed in patients with LS.[8,12] Development of a mouse LS model has been more complicated. *OCRL* knockout (KO) mice have no overt phenotype, ostensibly because they express high levels of INPP5B, another phosphatidylinositol 5′-phosphatase that apparently compensates for some OCRL functions.[13–15] INPP5B in the PT of mice is expressed at higher levels and with different splice variants compared with humans.[16] Because global KO of both *Ocrl* and *Inpp5b* in mice is lethal,[17,18] an LS mouse model was generated by crossing *Ocrl* KO mice that overexpress human INPP5B with a mouse *Inpp5b* KO: the resulting male mice exhibited modest proteinuria and aminoaciduria starting at 8 weeks of age.[19,20] A more recent mouse model has been described where *Inpp5b* was conditionally inactivated in the kidney of *Ocrl* KO mice.[21] PT cells in these mice expressed reduced levels of megalin and showed profoundly impaired endocytosis. Surprisingly, proteinuria was not observed immediately after KO, but rather required several months to develop. This temporal lag is inconsistent with a direct effect of OCRL on endocytic pathway function and suggests that additional changes that occur over longer time periods contribute to the LS phenotype. Additionally, the need to target both *Ocrl* and *Inpp5b* to observe any renal phenotype complicates the effort to pinpoint the specific role(s) of OCRL in PT function.

To investigate how loss of OCRL affects PT function, we generated chronic CRISPR/Cas9 *OCRL* KO and acute siRNA knockdown models of LS in PT cells. Strikingly, in all of our models, as well as in patient fibroblasts, we observed that loss of functional OCRL lengthened the duration of cell division and caused the accumulation of multinucleated cells. These effects were rescued upon expression of wild-type (WT), but not disease-causing mutants, of OCRL. Consistent with our previous studies, we found no defect in constitutive or flow-regulated endocytosis in these cells.[22–24] Careful examination of *ocrl* mutant zebrafish revealed that the length of the megalin (*lrp2*)-expressing segment of the pronephric kidney was reduced. This effect was phenocopied by morpholino (MO)-based knockdown of *ocrl*. We propose that impaired cell division during development and/or repair after injury lead to shorter PTs in patients with LS, resulting in reduced recovery of filtered proteins, ions, and other molecules by the PT. Mathematic modeling suggests that a reduction in the length of human PTs can account for the urinary excretion profile of albumin and LMW proteins (LMWPs) of patients with LS. Our data suggest a comprehensive new model for how impaired development and/or repair of the PT contribute to LMW proteinuria and transport defects in LS. Moreover, dynamic remodeling of nephron segment length by physiologic, pharmacologic, or dietary maneuvers provides a possible approach to slow kidney disease progression in patients with LS.

Significance Statement

Patients with Lowe syndrome (LS) develop abnormalities in proximal tubule function that cause declining kidney function. Mutations in the *OCRL* gene encoding cause LS. The enzyme encoded by *OCRL* hydrolyzes phosphatidylinositol 4,5-bisphosphate, a lipid that regulates myriad cellular functions. The authors created a knockout model of OCRL in human proximal tubule cells and observed that loss of OCRL impairs cell proliferation and results in the accumulation of multinucleated cells. *Lrp2*-positive segments of the pronephric kidney were shorter in *ocrl* mutant and morphant zebrafish. The authors also created a mathematic model that explains how loss of functional OCRL can lead to the kidney manifestations of LS. The authors hypothesize that impaired cell proliferation results in a shorter proximal tubule in patients with LS and that this contributes to proteinuria.

METHODS

Cell Culture

All cell culture reagents were from Sigma unless otherwise specified. HK-2 cells (RRID:CVCL_0302; *Homo sapiens*, adult male, cortex/PTs, papilloma immortalized) were obtained from ATCC. The cells were cultured in DMEM/F12 with 5 μg/ml insulin, 0.02 μg/ml dexamethasone, 0.01 μg/ml selenium, 5 μg/ml transferrin, 2 mM L-glutamine, and 10% FBS (Atlanta Biologicals). Human control fibroblasts and fibroblasts from patients with LS were obtained from Dr. Robert Nussbaum and cultured in DMEM with 2 mM L-glutamine and 10% FBS. Conditionally immortalized mRPTC cells (*Mus musculus*) were provided by Dr. Roy Zent and cultured in DMEM/F12 with 5 μg/ml insulin, 50 ng/ml hydrocortisone, 5 μg/ml selenium, 5 μg/ml transferrin, 6.5 ng/ml triiodothyronine, 2 mM L-glutamine, 2.5% FBS, and 92 μg/ml

D-valine, as described.[25] RPTEC/TERT1 cells (RRID:CVCL_K278; *H. sapiens*, adult male, cortex/PTs, hTERT immortalized) were obtained from ATCC and cultured in DMEM/F12, 5 pM triiodothyronine, 10 ng/ml human EGF, 5.0 μg/ml ascorbic acid, 5.0 μg/ml insulin, 25 ng/ml PG E_1 (EMD Millipore), 25 ng/ml hydrocortisone, 8.65 ng/ml sodium selenite, 0.1 mg/ml G418 (Corning), and 1.2 g/L sodium bicarbonate (Thermo Fisher Scientific).

Antibodies

Mouse monoclonal OCRL antibody (1:5 western blot) was a gift from Drs. Robert Nussbaum and Sharon Suchy.[26] Western blotting primary antibodies also included mouse monoclonal actin antibody (1:5000 of approximately 2 mg/ml stock, A1978; Sigma) and rabbit polyclonal INPP5B antibody (1:500 of approximately 0.8 mg/ml stock, 15141–1-AP; ProteinTech). Western blot secondary antibodies used were ECL Mouse IgG, HRP-linked whole Ab (1:5000, NA931; GE Healthcare) and ECL Rabbit IgG, HRP-linked whole Ab (1:5000, NA934; GE Healthcare). Primary cilia were labeled using mouse monoclonal anti-acetylated tubulin antibody (1:400 of approximately 1 mg/ml stock, T7451; Sigma) followed by goat anti-mouse Alexa Fluor 568 conjugated antibody (1:500 of a 2 mg/ml stock, A11031; Invitrogen).

CRISPR/Cas9 *OCRL* KO Clones

CRISPR/Cas9 KO clones were generated using modifications of the approach described previously.[27] A single guide RNA (sgRNA) targeting exon 13 of *OCRL* was selected using the CHOPCHOP design tool[28] (Supplemental Table 1). Although no off-target effects were found *via* CHOPCHOP, NCBI nucleotide BLAST of our sgRNA sequence against the GRCh38.p2. edition of the human genome was completed for a more conservative assessment. Blastn was used to identify any similar sequences with intact PAM sequences. We found no important potential off-target effects; top hits are listed in Supplemental Table 2. Standard desalted oligos obtained from Integrated DNA Technologies were subcloned into the pX330 CRISPR/Cas9 plasmid (Addgene). The forward and reverse oligos were first phosphorylated and annealed as follows: 1 μl of each oligo (100 μM), 1 μl of 10× T4 ligation buffer (New England Biolabs), 6.5 μl ddH_2O, and 0.5 μl T4 PNK (New England Biolabs) with a thermocycler setting at 37°C for 30 minutes, then 95°C for 5 minutes and ramping down to 25°C at 5°C/min. The annealed oligo duplexes were cloned into the pX330 vector in a single-step digestion ligation reaction containing 100 ng pX330, oligo duplex (1:150 dilution), 1 μl FastDigest BbsI (Thermo Fisher Scientific), 0.5 μl T7 DNA ligase (New England Biolabs), and ddH_2O in a total volume of 20 μl with thermocycler settings at 37°C for 5 minutes and 23°C for 5 minutes (six cycles total).

The same sgRNA sequence with added PAM sequence for nuclease binding/activation (Supplemental Table 1) was inserted into the pHRS surrogate reporter plasmid (PNA Bio Inc.). The forward and reverse oligos were phosphorylated and annealed as described in the previous paragraph for pX330 plasmid subcloning. The pHRS plasmid was digested with *Eco*R1-HF (New England Biolabs) and *Bam*[1]H-HF (New England Biolabs) in CutSmart Buffer (New England Biolabs) at 37°C for 30 minutes and purified after agarose gel electrophoresis using the Wizard SV Gel and PCR Clean-Up System (Promega) according to the manufacturer's protocol. Annealed oligo duplexes (1:250 dilution) were ligated into the purified pHRS vector using T7 DNA ligase at ambient temperature for 30 minutes according to the manufacturer's protocol. To prevent unwanted recombination products, ligation products of both pX330 and pHRS were treated with PlasmidSafe ATP-dependent DNase (Epicentre) at 37°C for 30 minutes.

Cleaned ligation products (2.5 μl) were transformed into One Shot Stbl3 Chemically Competent *E. coli* (Thermo Fisher Scientific) according to the manufacturer's protocol. Transformation products were seeded onto ampicillin (pX330) or kanamycin (pHRS) LB agar plates and cultured overnight. Plasmids were isolated and purified using the QIAprep spin Miniprep Kit (Qiagen) and the QIAGEN Plasmid Maxi Kit (Qiagen) according to the manufacturer's protocol. Oligonucleotide incorporation was confirmed by Sanger sequencing through the University of Pittsburgh Genomics Research Core using the hU6 (pX330) and pCMV (pHRS) forward sequencing primers. Sequencing data were analyzed using CLC Genomics Workbench (Qiagen).

Approximately 6×10^5 HK-2 cells were seeded in six-well plates and immediately transfected with 2.5 μg each of pX330 and pHRS plasmids per well using 6 μl Lipofectamine 3000 (Invitrogen), 10 μl P3000 reagent, and 0.5 ml OptiMEM according to the manufacturer's protocol. Growth medium was changed 12 hours after transfection and cells were grown for 48–72 hours with one medium change per day. Cells were then trypsinized with TrypLE Select (Thermo Fisher Scientific) for 10 minutes, centrifuged at 800 × *g* for 3 minutes, and resuspended in PBS supplemented with 10% FBS. Suspended cells were passed through a 50-μm Falcon filter (BD Biosciences) to ensure single-cell suspension. Cells were analyzed and sorted in a BD FACSAria II (BD Biosciences), with FACSDiva version 8 software. GFP was detected using the 488-nm blue laser with 505LP mirror and the 530/30BP filter; RFP was detected using the 488-nm blue laser with 595LP mirror and 610/20BP filter. RFP/GFP double-positive cells were collected in growth medium in 96-well plates to isolate clonal populations.

Clonal cells were lysed using 2× lysis buffer containing 5% β-mercaptoethanol, and analyzed for OCRL expression by western blot. Clones with no detectable OCRL expression were subjected to T7 endonuclease and sequencing analyses to confirm genomic editing. Genomic DNA was extracted from approximately 1×10^5 cells using QuickExtract DNA extraction solution (Epicentre) according to the manufacturer's protocol.

For sequencing analysis, extracted clonal DNA was amplified by PCR using GoTaq Green Master Mix (Promega) for a

50-μl reaction using 5 μl genomic DNA. The same primer sequences and touchdown PCR thermocycler settings were used as above in the T7 assay methods. Products were electrophoresed on a 1% agarose gel and purified using the Wizard SV Gel and PCR Clean-Up System, then ligated into the pGEM-T Easy Vector Systems plasmid (Promega). The ligation product was transformed into MAX Efficiency DH5α Competent Cells (Invitrogen) according to the manufacturer's protocol. Transformation products were seeded onto ampicillin LB agar plates (100 μl). Plasmid isolation and purification were performed using the QIAprep spin Miniprep Kit. Fifteen separate isolated plasmids for each clone were sequenced using Sanger Sequencing performed by the University of Pittsburgh Genomics Research Core using the T7 forward sequencing primer. Mutation analysis was completed using CLC Genomics Workbench.

Although HK-2 cells were isolated from a male human kidney, two different *OCRL* mutations were found in the genomic sequence of each of our two isolated clonal cell populations, leading to frameshifts and early termination of the protein. CRISPR/Cas9 editing of another X-linked gene in this cell line also required mutagenesis of two independent alleles, suggesting that HK-2 cells may have a duplicated X-chromosome (A. Labilloy, unpublished results). Consistent with this, DAPI staining of chromosome spreads revealed a range of 53–56 chromosomes in parental HK-2 cells (M. Gliozzi, unpublished results).

siRNA Transfection

Cells were transfected using Lipofectamine RNAiMAX with siRNA constructs targeting *OCRL* or luciferase as a control. A new siRNA oligonucleotide (construct 1) targeting *OCRL* was used in all studies except in rescue experiments (Supplemental Table 1). For rescue experiments, a previously characterized oligonucleotide and appropriate siRNA-resistant *OCRL* construct (construct 2) were used[22] (Supplemental Table 1). Both *OCRL* target sequences were purchased from GE Dharmacon. The control luciferase siRNA was purchased from Sigma. Cells were transfected twice for each experiment with 1 μg siRNA and 1.5 μl Lipofectamine RNAiMAX reagent in OptiMEM: first during plating and again approximately 24 hours later. Experiments were performed up to 4 days after initial transfection. Duplicate samples of transfected cells were solubilized to assess the efficiency of knockdown by western blotting.

Quantitation of Cell Multinucleation

Approximately 1×10^5 HK-2 cells transfected with siRNA or HK-2 CRISPR/Cas9 clonal cells, were plated on 12-mm coverslips, cultured for 3–4 days, then incubated with 10 μg/ml Alexa Fluor 647–conjugated wheat germ agglutinin (Thermo Fisher Scientific) and fixed with 4% paraformaldehyde. Coverslips were mounted onto glass slides using ProLong Gold antifade with DAPI (Thermo Fisher Scientific), imaged using a Leica DM6000 B microscope, and random fields acquired using a $\times$40 objective, 1.25–0.75 NA. The numbers of mono-, bi-, and multinucleated cells with clearly visible cell borders were counted in each image. Studies in siRNA-transfected mRPTC and RPTEC/TERT1 cells and in fibroblasts from patients with LS and control fibroblasts were conducted and analyzed in the same manner, except that 2×10^5 cells were plated per coverslip.

OCRL Rescue Experiments

Approximately 1×10^5 HK-2 cells were transfected with 1 μg plasmid DNA containing GFP-tagged empty vector (pGFP-N1), WT OCRL-GFP (pEGFP-C1), or G304E mutant OCRL-GFP (pEGFP-C1) constructs[22] and plated on 12-mm coverslips. Lipofectamine 2000 was used for transfection according to the manufacturer's protocol. Medium was changed daily. HK-2 cells were treated with siRNA for 2 days after the initial transfection. CRISPR/Cas9 clonal cells were cultured for 3 days, whereas siRNA treated HK-2 cells were cultured for 4 days. Coverslips were incubated with 10 μg/ml Alexa Fluor 647–conjugated wheat germ agglutinin on ice; fixed with 4% paraformaldehyde; mounted onto glass slides using ProLong Gold antifade with DAPI; imaged using a Leica DM6000 B microscope using a $\times$40 objective, 1.25–0.75 NA; and fields containing GFP-positive cells acquired. For each condition, the numbers of mono-, bi-, and multinucleated GFP-positive cells with clearly visible cell borders were counted in each image.

Time-Lapse Imaging of Cell Division

HK-2 CRISPR/Cas9 *OCRL* KO cells were plated sparsely on a 35×10-mm^2 glass-bottomed dish (MatTek) and cultured for approximately 12 hours. Random fields were selected and then imaged every 30 minutes overnight using a Leica TCS SP8 confocal microscope using a DIC setting with a $\times$40 objective, 1.30 NA. Additional experiments were conducted where control and *OCRL* KO cells were incubated with 5 μM Draq5 (Thermo Fisher Scientific) for 10 minutes according to manufacturer's instructions to elucidate nuclei. These experiments were imaged every 15 minutes for 5.75–11.25 hours using a Leica TCS SP8 confocal microscope using a combination of confocal and transmitted light settings with a $\times$40 objective, 1.10 NA. Metaphase length was assigned on the basis of the presence of chromosomes aligned in a single column. The initiation of anaphase was classified by a separation of chromosomes or, in cases where visualizing DNA content was difficult, the furrowing of cell membrane. The end of cytokinesis was determined by the formation of a nuclear structure in daughter cells, the complete shift in cell morphology from rounded to spread, and the absence of any noticeable cytokinetic bridge. When possible, cells were followed beyond the determined end of division to further ensure that cell division was completed. Images were analyzed in FIJI.

For time-lapse imaging of apoptotic cells, control and *OCRL* KO cells were plated at equal cell counts (10,000–25,000 cells per quadrant) on two quadrants of a split glass-bottom dish and cultured for approximately 12 hours. Cells were incubated with 5 μM NucView 488 Caspase-3 substrate (Biotium)

for 30 minutes and 5 μM Draq5 for 3 minutes in PBS at 37°C. Cells were washed twice in PBS and 250 μl culture medium was added per quadrant for imaging. Random fields from approximately equally dense locations in control and *OCRL* KO quadrants were selected and imaged every 20 minutes for 4.7–11.3 hours using a Leica TCS SP8 confocal microscope using a combination of confocal and DIC setting with a ×40 objective, 1.30 NA. Only cells that developed positive NucView staining during the imaging process were counted. Images were analyzed in FIJI.

FACS Sorting of CRISPR/Cas9 *OCRL* KO Cells

FACS sorting on the basis of cell nuclear ploidy was performed using modifications of the approach described by Duncan et al.[29] Cells recovered from a stock plate were resuspended (2×10^6 cells per ml) in phenol red–free culture medium and incubated with 15 μg/ml Hoechst 33342 (Sigma) and 5 μM reserpine (Invitrogen) for 30 minutes at 37°C. Cells were then incubated on ice with 5 μg/ml propidium iodide (Invitrogen) before FACS analysis and sorting in a FACS Aria II-SORP (BD Biosciences) using a 130-μm nozzle and DiVa v8.0.2 software. Dead and aggregated cells were removed on the basis of propidium iodide incorporation and pulse width analysis, respectively. Cells were sorted into 2C and >2C ploidy populations on the basis of DNA content measured using a violet 405-nm laser and 450–50-nm bandpass filter. An unsorted population was collected as a control. Cells were collected in medium containing 50% FBS and the cultures were supplemented for the next 5 days with penicillin-streptomycin (Gibco).

Mathematic Modeling of Protein Reabsorption

A mathematic model describing protein reabsorption along the human PT was created in MATLAB (MATLAB R2017a with ode45 solver). This model represents an adaptation of Lazzara and Deen's published model of albumin reabsorption that used experimental parameters obtained from rat studies.[30] The equation that describes uptake in a straight tubule with no differences in uptake capacity along the length and neglecting any resistance of radial mass transfer is:

$$\frac{dC}{dz} = \frac{-2}{uR}\left(\frac{V_{max}C}{K_m + C}\right) - \frac{C}{u}\frac{du}{dz},$$

where C is the concentration of protein in the tubule and u is the axial velocity of the filtrate.

The definition of axial velocity is on the basis of an exponential flow profile[31,32]:

$$Q(z) = Q_0 e^{(-wz)},$$

where Q is the volume flow in the PT. The change in volume flow per unit length, w, can be estimated on the basis of tubule length, L, and the normal fractional reabsorption of water, f_w:

$$Q(L) = (1 - f_w)Q_0 = Q_0 e^{(-wL)}.$$

Therefore,

$$w = \frac{-\ln(1 - f_w)}{L}.$$

The average axial velocity can be defined as:

$$u(z) = \frac{Q(z)}{\pi R^2}.$$

Therefore,

$$u(z) = u_0 e^{-wz} \text{ and } \frac{du}{dz} = -u_0 w e^{-wz}$$

with

$$u_0 = \frac{SNGFR}{\pi R^2}.$$

We have previously demonstrated that endocytic uptake in PT cells is flow dependent.[23,24] We assume that the reabsorptive capacity of the PT, V_{max}, varies with axial velocity. The simplest form in which to include a flow component in V_{max}, such that V_{max} is not zero in the absence of flow, is with the addition of a linear term so that V_{max} has the form:

$$V_{max} = V_{max0}(1 + \alpha \times u),$$

where V_{max0} is the basal uptake capacity in the absence of flow, α is 1 $s\cdot mm^{-1}$, and u has the units $mm\cdot s^{-1}$.

It is important to note, however, that the correlation between shear stress and uptake is unknown. We would expect the uptake capacity of the PT to decrease with decreasing flow, but without a quantitative assessment of the endocytic capacity and flow, we cannot conclusively define the relationship between V_{max} and fluid velocity.

Parameter Values Used to Model Albumin and LMWP Uptake along the Human PT

Default values for the parameters for human tubule length (L) and luminal radius were obtained from a published model of transport along the human nephron.[33] Values for fractional water reabsorption (f_w) and single nephron GFR (*SNGFR*) have also been previously determined.[30] The creatinine concentration in the tubule lumen increases according to the exponential water loss. We assume that the starting concentration of creatinine in the tubule lumen is equivalent to serum creatinine. Serum creatinine was estimated on the basis of reported values for children.[34] The protein concentration was divided by the creatinine concentration along the length of the tubule to give the protein-to-creatinine ratio (mg/mmol).

The specific trafficking rates of megalin trafficking in PT cells are unknown, so we relied on the published half-saturation concentration for albumin reabsorption ($K_{m,A}$).[35] Our estimate of the concentration of albumin entering the tubule (A_0) was on the basis of a sieving coefficient of 0.00062[36] and

plasma levels of 3.5 g/dl.[37] We believe that this is a more accurate estimate than the human albumin sieving coefficient calculated by Norden and colleagues on the basis of measurements of urinary albumin in patients with Dent disease.[38] That study assumed that no albumin is reabsorbed by the PT, whereas our data suggest that endocytic capacity may not be impaired in LS PT cells. The V_{max} was fit on the basis of the reported fractional reabsorption values for albumin, so that the fraction of A_0 that is remaining in the lumen at the end of the tubule is $(1-f_A)$.[30] Specifically, V_{max0} was adjusted to minimize the difference between the model at z=17 mm and the normal excretion ($[1-f_A]\times A_0$). Using these parameters, the resulting basal uptake capacity, V_{max0}, is 0.039 ng/s per mm^2, and the average value of V_{max} over the length of the tubule with a normal SNGFR is 0.065 ng/s per mm^2, which is similar to that in the rat model (0.086 ng/s per mm^2).[30]

The concentration of LWMP entering the tubule ($LMWP_0$) was estimated on the basis of the finding that approximately 3.1 times as much LMWP enters the PT as albumin.[36] Fractional LWMP reabsorption (f_{LMWP}) was estimated on the basis of normal fractional reabsorption of RBP.[39] On the basis of our assumption that megalin trafficking rates do not depend on binding of ligands to the receptor, we can use the same V_{max} for both albumin and LMWP. This V_{max} was used in the LMWP model and the reabsorption $K_{m,LMWP}$ was fit because we lack an estimate for the reabsorption half-saturation concentration for LMWPs. Again, the model was fit so that the fraction of $LMWP_0$ that is remaining in the lumen at the end of the tubule is $(1-f_{LMWP})$. The resulting $K_{m,LMWP}$ is 10.4 μg/ml. The f_A in patients with LS (0.86) was set such that albumin excretion was ten-fold higher than normal and the f_{LMWP} in LS (0.7) was set such that the LMWP excretion was 1000-fold higher than normal, as determined by urinary excretion measurements.[2,40] Table 1 provides the parameters used in the final model.

Table 1. Parameter values used to model albumin uptake along the human PT

Parameter	Value	Reference
Tubule length, L	17 mm	33
Tubule radius, R	18.5 μm	33
SNGFR	71 nl/min	30
Basal reabsorptive capacity, V_{max0}	0.039 ng/s per mm^2	[a]
Albumin concentration at half saturation, $K_{m,A}$	31 μg/ml	35
Initial filtrate albumin concentration, A_0	21.7 μg/ml	36,37
LMWP concentration at half saturation, $K_{m,LMWP}$	10.4 μg/ml	[a]
Initial filtrate LMWP concentration, $LMWP_0$	67.3 μg/ml	36
Initial filtrate creatinine concentration	0.5 mg/dl	34
Fractional water reabsorption, f_w	0.70	30
Fractional albumin reabsorption, f_A	0.986	30
Fractional LMWP reabsorption, f_{LMWP}	0.9997	39

[a]Indicates fit parameter.

Zebrafish Husbandry

Zebrafish were reared according to established protocols,[41] which were approved by the University of Pittsburgh Institutional Animal Care and Use Committee.

Zebrafish Injections, Crosses, and Whole Mount *In Situ* Hybridization

The validated zebrafish *ocrl* MO, which translationally blocks *ocrl* transcripts, was synthesized by Gene Tools LLC (Philomath, OR) as previously described.[6] AB strain zebrafish one-cell embryos were injected with 6 ng or 8 ng *ocrl* MO into the yolk. *Ocrl*$^{+/-}$ heterozygous animals were gifted to us by Martin Lowe; generation of the mutant allele was previously described.[12] *Ocrl*$^{-/-}$ larvae were acquired by incrossing *ocrl*$^{+/-}$ animals. All embryos developed at 28°C for 3 days in E3 embryo medium containing 30 μg/ml phenylthiourea to inhibit pigment deposition. Larvae were fixed in 4% paraformaldehyde/phosphate buffer solution overnight at 4°C.

A megalin/*lrp2a* fragment was PCR amplified (500 bp) from genomic DNA with the following primers adding a T3 promoter in antisense: forward 5′-CGAGGGCCACGTTTACTGGACGACT-3′ and reverse 5′-GGATCCAATTAACCCTCACTAAAGGGTGTCAATGAAGGACACCCCG-3′. The *clcnk* cDNA sequence (approximately 2.4 kb) was cloned into pBluescript antisense to a T7 promoter. A *cdh17* clone (synthetically generated by Eurofins) containing the *cdh17* sequence, 255 bp of the end of the coding sequence, and 195 bp of 3′UTR; the reverse *cdh17* sequence was cloned with a SP6 prior and *Nhe*I restriction site afterwards into a pCR2.1 vector. DIG antisense probes for *lrp2a*, *clcnk*, and *cdh17* were generated using the appropriate RNA polymerase and DIG RNA Labeling Mix (Roche). Whole mount *in situ* hybridization with DIG antisense RNA probes was conducted as described previously.[42] Animals probed for *lrp2a* and *cdh17* were deyolked mechanically with forceps. *In situ* images were captured on a Leica MZ16 Stereomicroscope with a QImaging Retiga 1300 camera and QCapture Suite 2.98.2 software. After imaging, *ocrl*$^{+/-}$ progeny were genotyped for *ocrl* mutant alleles by PCR amplification.[8]

Quantitation of Albumin Endocytosis

Approximately 3×10^5 CRISPR/Cas9 control and *OCRL* KO clonal cells were plated in μ-slide VI six-well ibi-treated chambers (Ibidi). Cells were cultured for 3 days with medium changes twice per day. For endocytosis assays, cells were incubated with 40 μg/ml Alexa Fluor 647-BSA (Thermo Fisher Scientific) for 1 hour at 37°C under static conditions or at 0.1 dyne/cm^2 FSS as previously described.[23] Cells were

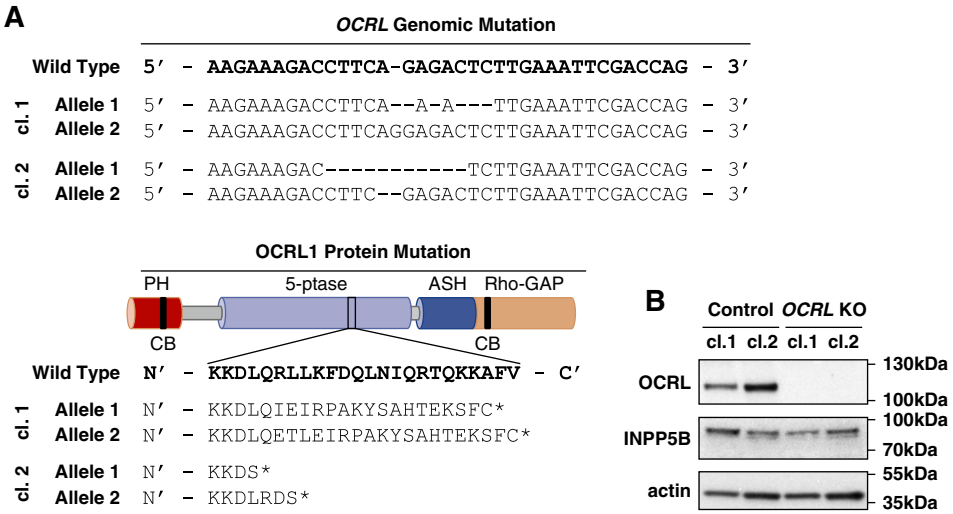

Figure 1. CRISPR/Cas9-generated *OCRL* KO clones in HK-2 cells. A CRISPR/Cas9 guide sequence was generated to target exon 13 (within the 5′-phosphatase domain) of *OCRL* in HK-2 cells. (A) Two separate KO clones (cl.1 and cl.2) were collected, each with insertion/deletion mutations causing a frameshift and protein truncation (asterisk) within the 5′-phosphatase domain. WT genomic DNA section correlates to nucleotides 129,565,848–129,565,883 in GRCh38.p7. WT protein sequence section correlates to amino acids 441–464. (B) Blotting with antibodies against OCRL, INPP5B, and β-actin confirms the absence of OCRL expression, with no compensatory increase in INPP5B expression in either CRISPR/Cas9 KO clone.

washed, fixed in 4% paraformaldehyde, and imaged using a Leica TCS SP5 confocal microscope using a ×40 objective, 1.25 NA. Five confocal stacks were acquired per condition and the intensity of maximum projections was quantified in FIJI after background subtraction.[23]

Because of technical challenges in generating efficient siRNA-mediated knockdown in Ibidi chambers, we measured endocytosis in siRNA-treated cells plated on Transwell filter supports. HK-2 cells (5×10^5) were plated on 12-mm Transwell with 0.4-μm pore polycarbonate membrane inserts (Corning) in a 12-well plate, with 0.5 ml apical medium and 1.0 ml basolateral medium. Cells were treated with siRNA as described in the siRNA transfection section. Cells were cultured for 4 days on an orbital shaker at approximately 74 rpm with daily medium changes. We have previously demonstrated that chronic exposure to orbital shear stress enhances cell proliferation and differentiation.[24] To measure endocytosis under static conditions, filters were transferred to static conditions the night before the experiment. All cells were incubated with 40 μg/ml Alexa Fluor 647-BSA for 1 hour at 37°C under static conditions or orbital shear stress as indicated. Cells were fixed in 4% paraformaldehyde and mounted using ProLong Gold antifade with DAPI. Imaging and analysis were completed in the same manner as described for the CRISPR/Cas9 clones above. In both CRISPR/Cas9 clonal and siRNA experiments, albumin uptake under static conditions was normalized to 1 for each cell population and the fold increase in albumin uptake upon exposure to FSS was calculated.

Measurement of Cilia Length

Approximately 5×10^5 HK-2 cells transfected with siRNA or HK-2 CRISPR/Cas9 clonal cells, were plated on 12-mm coverslips (Fisher Scientific) in a 12-well plate. Cells were cultured for 3 days with daily medium changes, serum-starved overnight in HK-2 medium without FBS, and then fixed in 4% paraformaldehyde. Cells were processed for indirect immunofluorescence using mouse anti-acetylated tubulin (1:400 of approximately 1 mg/ml stock, T7451) and Alexa Fluor 568–conjugated goat anti-mouse secondary antibody (1:500 of a 2 mg/ml stock, A11031). Coverslips were mounted onto glass slides with ProLong Gold antifade with DAPI. Random fields for each condition were imaged using a Leica DM6000 B microscope using a ×40 objective, 1.25–0.75 NA, and analyzed in FIJI. Cilia were measured by tracing using the freehand drawing tool. The same drawing tool was used to measure 10 μm from a scaled image to normalize measurements.

Statistical Analysis

Statistical significances of all data were assessed using Prism 7 (GraphPad).

RESULTS

OCRL Depletion Leads to Accumulation of Multinucleated Cells

We used CRISPR/Cas9 genome editing to isolate two HK-2 *OCRL* KO clones containing indels within the 5′-phosphatase domain of OCRL (Figure 1A). As controls, we isolated two HK-2 clones after transfection with empty vector. OCRL was readily detected by western blotting of control HK-2 cell clones using an antibody directed against the amino terminus

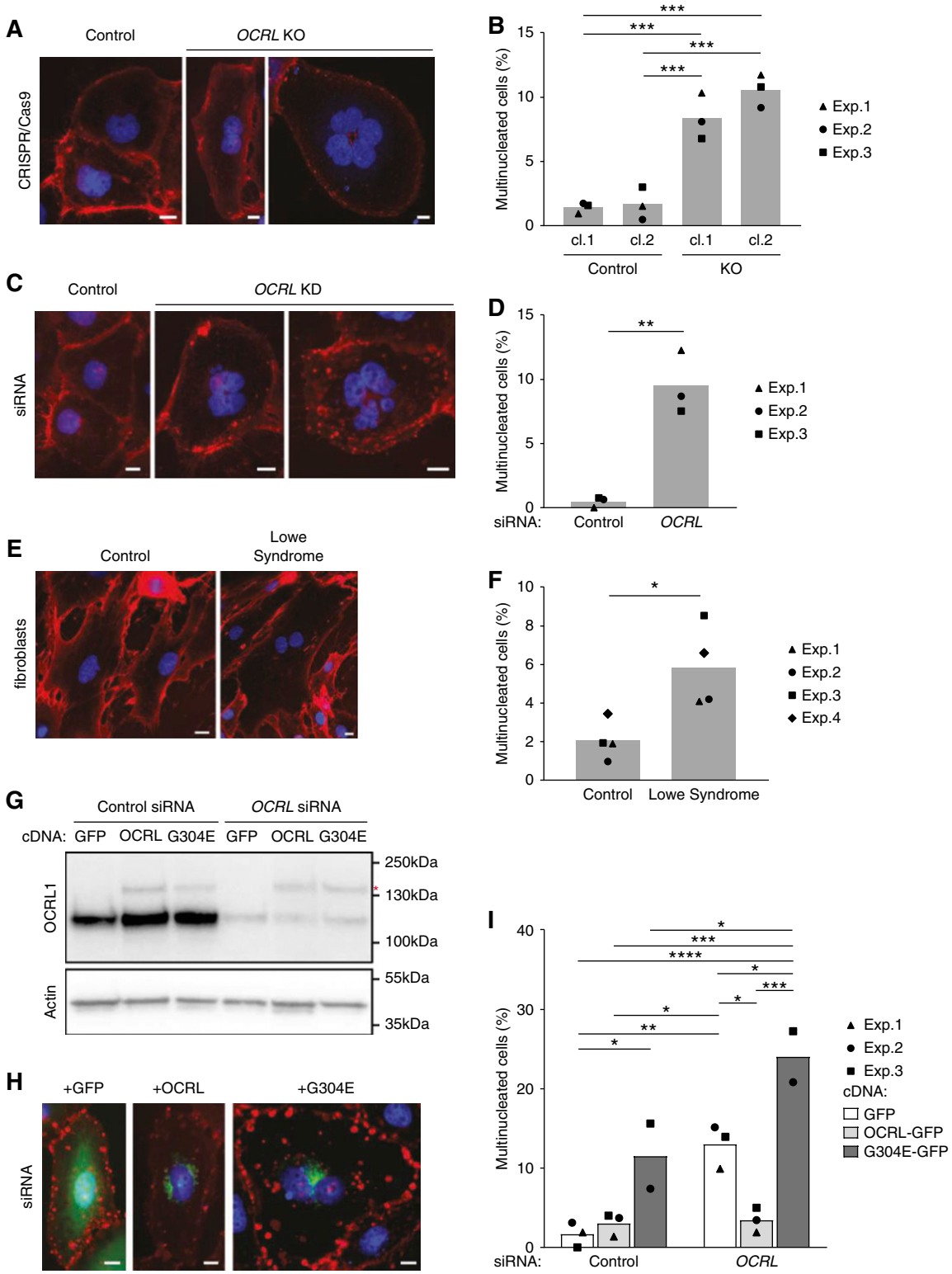

Figure 2. Cells lacking OCRL exhibit increased multinucleation. Control and OCRL-depleted cells were stained with fluorescently conjugated wheat germ agglutinin (red) and DAPI (blue) to visualize cell borders and nuclei, respectively. (A) Representative images of mononuclear cells in control CRISPR/Cas9 clones and multinucleated cells in CRISPR/Cas9 *OCRL* KO clones. (B) The percentage of HK-2 cells with multiple nuclei is plotted (mean and individual points of three independent experiments; 69–394 cells per condition scored in each experiment). (C) Representative images of mononuclear cells in cells transfected with control siRNA and multinucleated cells in cells transfected with *OCRL* siRNA. (D) The percentage of cells with multiple nuclei is plotted (mean and individual points of

of the protein (Figure 1B). No band was observed at the predicted location corresponding either to the full length (approximately 97 kDa; Figure 1B) or to the expected truncated protein (approximately 51 kDa) in the *OCRL* KO clones (Supplemental Figure 1). There was no compensatory increase in INPP5B levels in our *OCRL* KO clones (Figure 1B).

In characterizing our CRISPR/Cas9 clones, we noticed that our *OCRL* KO clones exhibited reduced proliferation rates compared with control clones. Quantitation of cell nuclei in *OCRL* KO cells or in siRNA-transfected cells revealed a 22%–31% decrease in nuclei per field in OCRL-depleted cells compared with controls plated at identical densities (Supplemental Figure 2, A–D). There was no significant difference in the fraction of apoptotic cells in KO clones at steady state (Supplemental Figure 2E). To test whether cell division was impaired, we quantified the frequency of cells with multiple nuclei in our siRNA-transfected or *OCRL* KO models (Figure 2). Whereas <2% of cells in the control cell populations had more than one nucleus, approximately 10% of the *OCRL* KO clones (Figure 2, A and B) and *OCRL* siRNA transfected cells (Figure 2, C and D) were multinucleated. We attempted to quantify the frequency of PT cell multinucleation in hematoxylin and eosin–stained sections of kidney samples obtained from deceased patients with LS and age-matched controls, but the tissue quality was insufficient to reliably identify multinucleated cells (not shown). However, we did observe an increased fraction of multinucleated cells in primary fibroblasts from patients with LS (Figure 2, E and F) as well as upon siRNA knockdown of OCRL in two other PT cell lines derived from mice and humans (Supplemental Figure 3). Multinucleated cells contained up to four nuclei per cell (Figure 2, A and C), suggesting that errors in division can occur repeatedly in some cells. Heterologous expression of siRNA-resistant, GFP-tagged WT OCRL prevented the accumulation of multinucleated cells in *OCRL* siRNA-transfected cells (Figure 2, G–I). By contrast, transfection with a disease-causing mutant of OCRL (G304E)[22] increased the frequency of multinucleation in both control and *OCRL*-knockdown cells, likely reflecting a dominant-negative effect of overexpressing the mutant construct (Figure 2I). Expression of G304E in control and *OCRL* KO clones also increased multinucleation, but WT OCRL was unable to resolve preexisting multinucleation in cells (data not shown). Together, these data suggest that the impairment of cell division caused by OCRL depletion can be prevented, but that reexpression of OCRL does not resolve preexisting multinucleation in KO cells.

Impaired Cell Cycle Transit Leads to Accumulation of Multinucleated Cells

Time-lapse microscopy confirmed the defect in cytokinesis in an *OCRL* KO clone. Figure 3A shows frames taken 30 minutes apart documenting a tripolar cell division that resolved into two daughter cells, suggesting that one daughter cell retained two nuclei. Quantitation of the time spent in later stages of the cell cycle (metaphase through cytokinesis) revealed that *OCRL* KO cells had markedly prolonged stages of metaphase and/or anaphase/cytokinesis compared with control cells (Figure 3B, Supplemental Videos 1–3). Moreover, a delay in cell cycle transit time correlated with impaired mitotic outcomes, because multinucleated cells preferentially resulted from longer cell divisions (Figure 3C). To examine how proliferation, division, and death establish the equilibrium between cells having one versus more than one nucleus, CRISPR/Cas9 cell clones were sorted by FACS for nuclear content to isolate populations enriched for mononuclear (2C) or multinucleated (>2C) cells and followed over multiple passages (Figure 3D). The mononuclear-enriched cell population became progressively multinucleated, suggesting that a fraction of cells lacking OCRL exhibit defective cell division. By contrast, the fraction of multinucleated cells declined slightly in the >2C fraction (Figure 3D). By passage 10, the percentage of multinucleated cells in both populations had returned to that of the unsorted parental cells (approximately 12%).

Mathematic Model for the Effect of PT Length and Diameter on Albumin Uptake

Our data in CRISPR/Cas9 clones and siRNA-depleted PT cells suggest that an impairment in cell division results in reduced proliferation and an increased proportion of multinucleated cells in cell populations lacking functional OCRL. We hypothesize that changes in these set points during kidney development affect PT length and/or diameter and lead to the incomplete reabsorption of filtered proteins, ions, and metabolites characteristically observed in LS. Analysis of urinary protein profiles in patients with LS reveals a ten-fold increase in albumin excretion and an approximately 1000-fold increase

three independent experiments; 111–481 cells per condition scored in each experiment). (E) Wheat germ agglutinin and DAPI were used to visualize cell borders and nuclei in control and LS fibroblast primary cultures. (F) The percentage of cells with multiple nuclei is plotted (mean and individual points in three independent experiments; 99–171 cells per condition scored in each experiment). (G) OCRL-depleted cells were transfected with cDNAs encoding GFP, or with siRNA-resistant GFP-tagged WT OCRL (OCRL) or LS-causing mutant OCRL-G304E (G304E). Efficient knockdown of OCRL (90%–95%) in these cells and heterologous expression of GFP-tagged OCRL and G304E (red asterisk) were confirmed by western blotting of cell lysates. (H) Representative expression patterns of each construct are shown (green). (I) The percentage of cells with multiple nuclei in cells treated with siRNA and expressing GFP, OCRL, and G304E is plotted (mean and individual points of three experiments for GFP and OCRL, two experiments for G304E; 11–146 cells per condition scored in each experiment). Scale bar (A, C, E, and G), 10 μm. *$P<0.05$, **$P<0.01$, ***$P<0.001$, and ****$P<0.001$ on the basis of a one-way ANOVA Tukey's multiple comparisons test in (B), unpaired *t* test in (D) and (F), and two-way ANOVA Tukey's multiple comparisons test in (I). cl, clone; Exp, experiment.

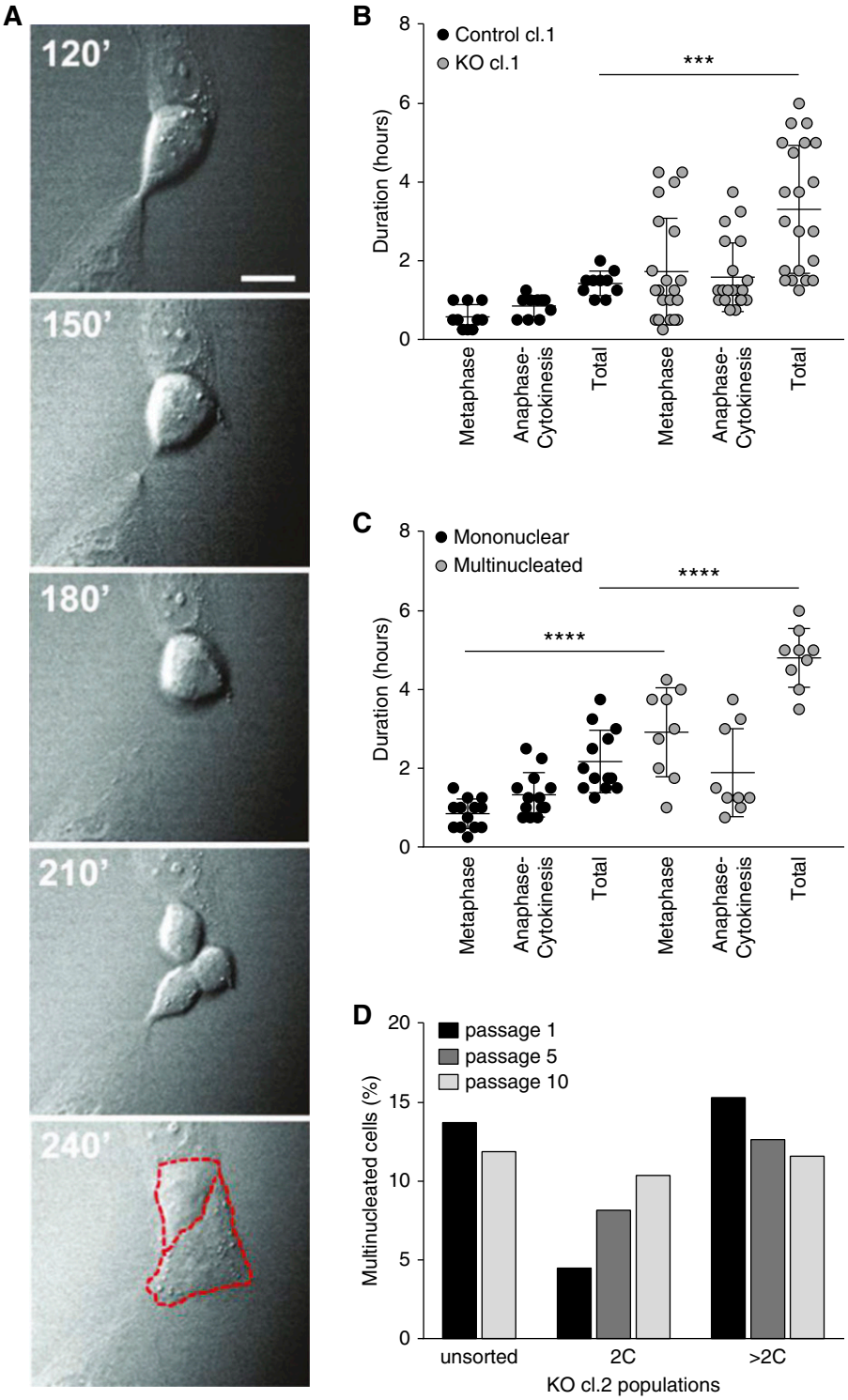

Figure 3. Multinucleated CRISPR/Cas9 *OCRL* KO cells result from prolonged cell cycle transit. (A) DIC imaging time course showing a tripolar division that resolves into two cells (borders highlighted in red, dashed lines) Scale bar, 25 μm. (B) CRISPR/Cas9 control clone 1 (cl.1) and KO cl.1 cells were imaged live every 15 minutes for 5.75–11.25 hours to capture cell divisions in randomly selected fields. The plot shows the durations of the metaphase and anaphase-cytokinesis stages of mitosis, and the total time spent in metaphase-cytokinesis measured in individual cells that underwent mitosis during the imaging period (control cl.1, 10 cells and KO cl.1, 23 cells). (C) Data from KO cl.1 cells in (B) were segregated on the basis of the outcome of mitosis (13 mononuclear versus nine multinucleated cells), and the durations of metaphase, anaphase-cytokinesis, and the total time spent in metaphase-cytokinesis for each are plotted. ***$P<0.001$ and ****$P<0.001$ on the basis of two-way ANOVA Holm–Sidak multiple comparisons

in LMWP excretion, on the basis of measurements of RBP.[2] To assess how changes in PT length might affect the uptake of filtered ligands, we adapted a published mathematic model on the basis of experimentally determined parameters in rodents[30] to incorporate best estimated values of tubule size, plasma albumin levels, and fractional reabsorption of albumin and LMW proteinuria in humans (Figure 4). Details of the model parameters and assumptions are provided in the Methods. The model predicts rapid initial albumin uptake in the tubule because concomitant water reabsorption maintains the albumin concentration above the estimated K_m. The fractional reabsorbance values in LS are estimated to be 0.86 for albumin and 0.7 for LMWP versus 0.986 and 0.9997 for normal, respectively. The model predicts that an approximately 30% decrease in PT length can account for the excess in urinary albumin and LMWP excretion in patients with LS (28.5% for albumin and 33.8% for LMWP; black arrows in Figure 4A). Reduced GFR has been reported in patients with LS, so we tested the effect of reducing the SNGFR in our model (Figure 4B). Reduced GFR is likely due in part to nephron dropout, and studies in rats demonstrate that SNGFR drops by only approximately 30% when whole kidney GFR is reduced by approximately 70%.[43] Our model predicts that a greater reduction in length would be required to result in the levels of urinary albumin and LMWP excretion observed in patients with LS as SNGFR is reduced. For example, a 20% reduction in SNGFR would necessitate a 36.2% reduction in PT length for albumin and 42.6% for LMWP (Figure 4B). Interestingly, changes in PT diameter had little effect on urinary excretion profiles under normal conditions or upon reduction in SNGFR, because this resulted in opposing effects on the flow-dependent reabsorptive capacity and residence time of filtered proteins in the PT lumen that tended to cancel out.

Because an endocytic defect has been observed in disease models of LS, we also modeled the effect of fractionally reduced PT reabsorptive capacity on albumin and LMWP clearance. As shown in Supplemental Figure 4, A and B, an approximately 30% reduction in V_{max} due to a decreased number of free megalin receptors in the PT could result in the urinary excretion profile observed in patients with LS. Similar to the predicted effects on changes in PT length, a 20% reduction in SNGFR would necessitate a 40%–45% reduction in V_{max} (Supplemental Figure 4, C and D). Because V_{max} in our model has a synergistic effect with shortened PT length, smaller reductions in each could also result in the proteinuria observed in LS.

Loss of OCRL Shortens Megalin/*lrp2a*-Expressing Segments in the Zebrafish Pronephric Kidney

To assess whether there is a functional consequence of impaired cell division on kidney segmentation, we examined PT length in *ocrl* mutant and morphant zebrafish using segment-specific markers. Megalin/*lrp2a* is selectively expressed in the PT segment,[44] whereas *cdh17* is expressed along the entire length of the pronephric kidney.[45,46] Using *in situ* hybridization, we measured the lengths of *lrp2a*- and *cdh17*-expressing segments in *ocrl* mutant ($ocrl^{-/-}$) and morphant zebrafish. *Ocrl* transgenic ($ocrl^{-/-}$) zebrafish exhibited a significant reduction in the *lrp2a*-expressing segment compared with WT ($ocrl^{+/+}$) and heterozygote ($ocrl^{+/-}$) control fish (Figure 5, A–D). By contrast, there was no difference in the length of the entire pronephric tubule quantified by *cdh17* expression (Figure 5, B–E). Overall, this resulted in the selective shortening of the PT of $ocrl^{-/-}$ fish by 17% relative to controls (Figure 5G). Injection of *ocrl* MO also resulted in a dose-dependent reduction in *lrp2a*-expressing segment lengths (Supplemental Figure 5, A and B), as well as in the entire *cdh17*-expressing tubule (Supplemental Figure 5, C and D). The effect on *lrp2a*-expressing segments was more pronounced, because the overall fraction of the pronephric tubule that was *lrp2a*-positive decreased in a dose-dependent manner (Supplemental Figure 5E).

To assess whether reduced PT length was compensated by elongation of other pronephric kidney segments, we measured the length of distal tubule (*clcnk*-expressing) segments in *ocrl* transgenic fish versus controls (Figure 5, C–F). We observed a slight increase in overall and fractional *clcnk* expression length in *ocrl* mutants, although this increase did not reach statistical significance (Figure 5, F–H). Together, our data suggest that OCRL plays a major role in development of the PT, and that *ocrl* depletion in zebrafish models of LS results in a reduction in PT length consistent with that predicted to result in tubular proteinuria.

Flow-Dependent Uptake in PT Cells Is Unaffected by *OCRL* KD

We previously found that PT cells rapidly adjust their endocytic capacity in response to acute changes in fluid shear stress.[23,24] Defective responses to changes in tubular flow resulting from defects in endocytic trafficking and/or in cilia-dependent flow sensing could contribute to the tubular proteinuria characteristic of LS. We quantified constitutive and flow-stimulated endocytic uptake of AlexaFluor 647 albumin in control and *OCRL* KO CRISPR/Cas9 clones, and in cells treated with control or *OCRL* siRNA (Supplemental Figure 6). Although individual CRISPR/Cas9 clones had different baseline levels of endocytic uptake, we found no consistent effect on constitutive endocytosis upon KO of *OCRL* by CRISPR/Cas9. Similarly, constitutive endocytosis in OCRL-depleted cells was similar to control, consistent with our previously published studies using a different siRNA oligonucleotide.[22] In all cases, exposure to FSS

test. (D) CRISPR KO clone 2 (cl.2) cells were sorted by FACS on the basis of nuclear content. Mononuclear (2C) and multinucleated (>2C) cells were isolated and cultured separately for ten passages. The percentage of cells with multiple nuclei was assessed at passages 1, 5, and 10 by fluorescence staining. cl, clone.

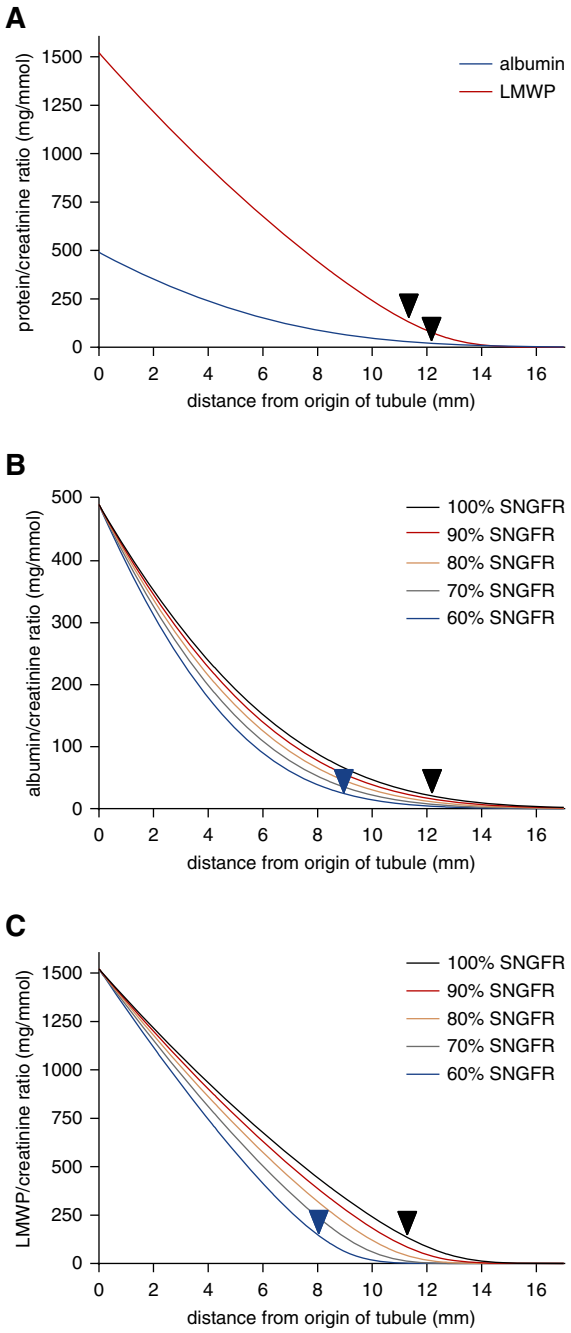

Figure 4. Mathematic model of albumin uptake along the PT. (A) Albumin-to-creatinine ratio (blue curve) and LMWP-to-creatinine ratio (red curve) along the human PT were modeled as described in the Methods. The models were fitted to the measured fractional reabsorbance in humans (0.986 for albumin and 0.9997 for LMWP) at the end of the tubule. In patients with LS, the estimated fractional reabsorptions for albumin and LMWP are 0.86 and 0.70, respectively. As denoted by the black arrows, an approximately 30% reduction in PT length is predicted to result in the tubular proteinuria phenotype characteristic of LS. The effects of reduced SNGFR on urinary excretion profiles of albumin (B) and LMWP (C) are plotted. A progressively greater reduction in PT length would be needed to produce the predicted urinary excretion profile as SNGFR declines from 100% to 60% of control.

resulted in an approximately 1.3-fold increase in albumin uptake, regardless of whether OCRL was expressed (Supplemental Figure 6).

Both shorter and longer cilia have been reported upon OCRL depletion in cells and zebrafish, and an emerging consensus is that effects on cilia length are irrelevant to LS pathology.[6,8,47] Similar to our previous observation in other cell types, acute knockdown of OCRL in HK-2 cells using siRNA increased mean cilia length (Supplemental Figure 7, A and B). However, cilia length was variably affected in individual CRISPR/Cas9 *OCRL* KO clones compared with control clones (Supplemental Figure 7, C and D). We conclude that loss of functional OCRL does not affect flow-dependent endocytic responses in PT cells.

DISCUSSION

Despite considerable study, the direct causes of tubular proteinuria and transport defects in patients with LS have remained elusive. Most studies to date have focused on a potential role for OCRL in maintaining efficient endocytosis of albumin and other filtered megalin/cubilin ligands by the PT. Our studies here suggest that reduced cell proliferation resulting from defective cytokinesis leads to selective shortening of megalin-expressing nephron segments. Mathematic modeling demonstrates that shortened PT lengths, within the range we measured in zebrafish, could account for the incomplete resorption of filtered ligands observed in patients with LS. Importantly, shorter PTs can also explain the other renal transport deficiencies commonly observed in these patients.

We found a consistent decrease in cell proliferation when we used either siRNA or gene-editing to deplete OCRL. Additionally, we observed a striking accumulation of multinucleated cells under these conditions. We also observed increased numbers of multinucleated cells in mouse PT cells depleted of OCRL and in primary cultures of human LS fibroblasts. Heterologous expression of functional OCRL prevented the accumulation of new multinucleated cells in siRNA experiments, suggesting that multinucleated cell formation is dependent on the absence of functioning *OCRL*. Interestingly, heterologous expression of a disease-causing mutant of OCRL resulted in accumulation of increased numbers of multinucleated cells. We hypothesize that a subset of OCRL mutants have dominant negative effects on cytokinesis that contribute to phenotypic variation in patients with LS.

We found that megalin/*lrp2a*-positive segment lengths in *ocrl* mutant and morphant zebrafish were shortened (by 17% in transgenic, 16% in 6 ng MO, and 42% in 8 ng MO) compared with the overall length of the pronephric kidney. Consistent with the decrease in PT segment length that we observed in transgenic and morphant zebrafish, our mathematic model for albumin uptake in humans[30] suggests that an approximately 30% decrease in PT length could account for the urinary protein excretion profile of patients with LS. Although

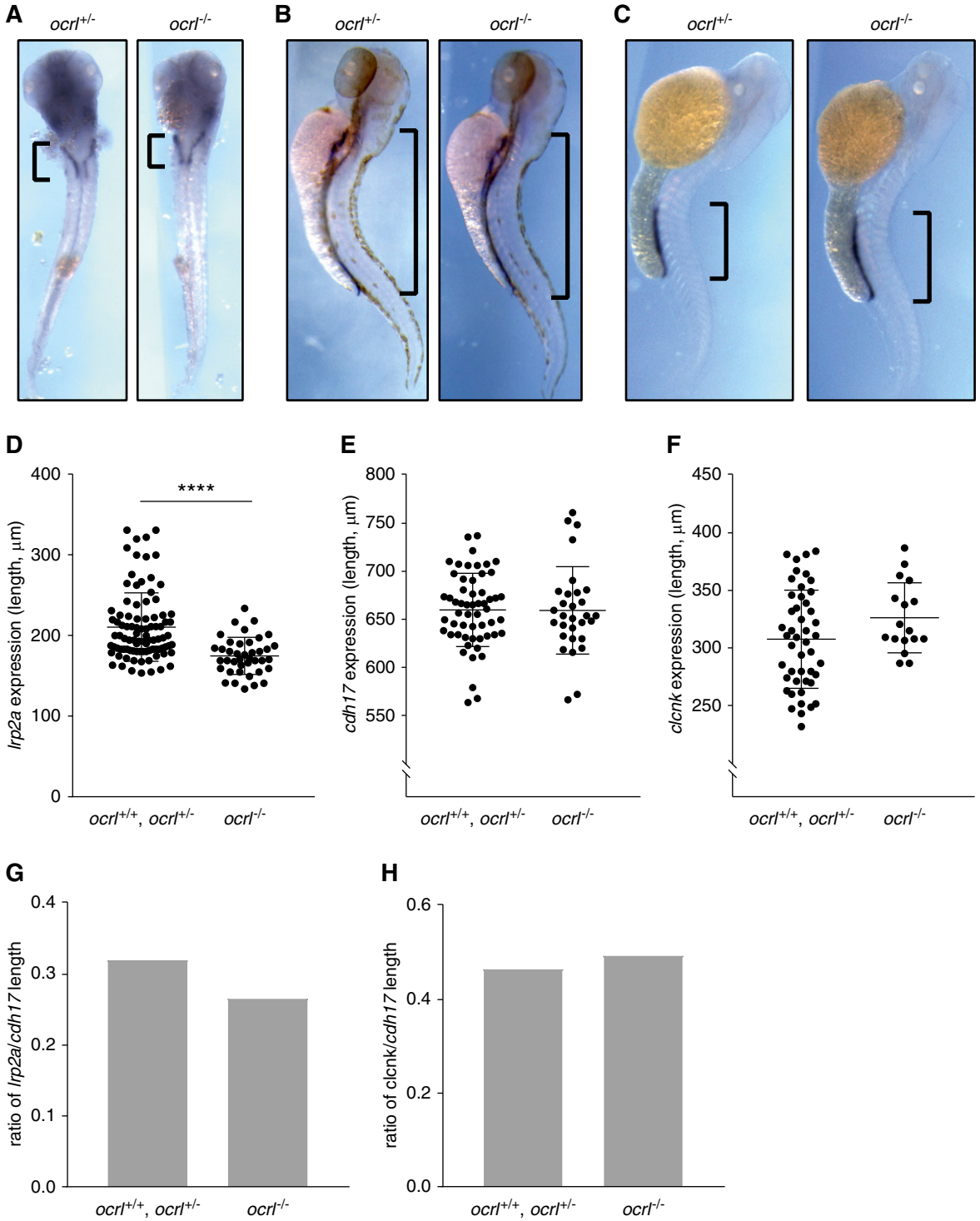

Figure 5. LS transgenic zebrafish have selectively shortened megalin/*lrp2a*-positive pronephric segments. *In situ* hybridization of megalin/*lrp2a* (PT marker) (A and D), *cdh17* (pronephric tubule marker) (B and E), and *clcnk* (distal tubule marker) (C and F) was performed in WT ($ocrl^{+/+}$), heterozygous mutant ($ocrl^{+/-}$), and homozygous mutant ($ocrl^{-/-}$) transgenic zebrafish at 72 hpf. The distributions of *lrp2a* (A), *cdh17* (B), and *clcnk* (B), and expression in representative zebrafish, are shown. Scatter plots show the lengths of *lrp2a*- (D), *cdh17*- (E), and *clcnk*- (E) positive segments measured in $ocrl^{+/+}$ and $ocrl^{+/-}$ zebrafish compared with $ocrl^{-/-}$ zebrafish (mean±SD; *lrp2a*, *n*=40–92; *cdh17*, *n*=33–56; *clcnk*, *n*=17–47). Ratios of average *lrp2a* (G) and *clcnk* (H) lengths over average *cdh17* length were compared among $ocrl^{+/+}$, $ocrl^{+/-}$, and $ocrl^{-/-}$ zebrafish. ****$P<0.001$ on the basis of an unpaired *t* test in (B).

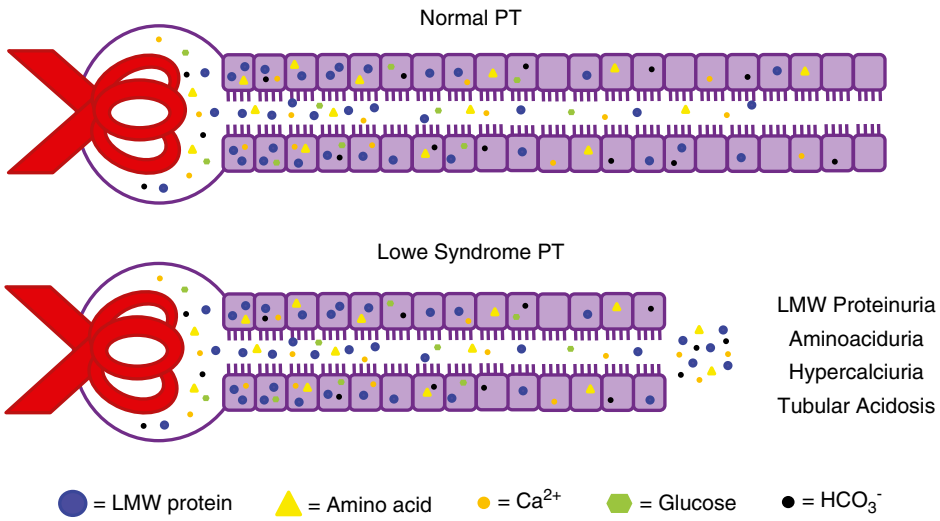

Figure 6. Model for how shortened PTs may explain kidney pathogenesis in LS. We hypothesize that defective cell division caused by lack of functional OCRL alters PT development or regeneration after injury, resulting in shorter (and/or narrower) PTs. Decreased PT reabsorption area can lead to incomplete reabsorption of LMWPs, and can also account for the aminoaciduria, hypercalciuria, and RTA characteristically observed in patients (see text for details). PTs have a high excess capacity for glucose uptake, so shorter PTs do not necessarily lead to glycosuria.

we detected potentially multinucleated cells in samples from patients with LS and in morphant zebrafish, definitive confirmation was technically very challenging. Using less rigorous criteria, the frequency of false positives made it impossible to reliably determine whether multinucleated cells are more prevalent in OCRL-deficient tissues. It is also possible that impaired cytokinesis within the geometric constraints of the pronephric kidney results simply in slower proliferation that affects PT growth.

Defective elongation of the PT due to impaired cytokinesis is consistent with the development of renal malfunction in patients with LS and in mice, and may contribute to the impaired proliferation of tubule-producing mesenchymal cells described in kidney-differentiated iPSCs derived from patients with LS.[48] Patients with LS typically develop LMW proteinuria during the first several months after birth. Studies of microdissected human PTs suggest that PTs grow rapidly in length for the first several months after birth.[49] At about 6 months of age, which roughly coincides with the onset of LMW proteinuria, PT diameters also begin to increase. Similarly, in a recently described mouse model for LS, LMW proteinuria was not immediately observed upon conditional KO of *Inpp5b* in the kidneys of 2-week-old *Ocrl*$^{-/-}$ mice, but rather took 1–3 months to develop.[21] This period occurs during an active stage of PT development, and, indeed, the PT is the only nephron segment in mice that increases in size between 2 and 12 months of age.[50] The slow onset of LMW proteinuria after acute KO of *Inpp5b* seems more consistent with a gradually forming defect in kidney architecture than with the sudden loss of a specific PT cell function.

In agreement with our previous studies, we found no evidence for a role of OCRL in endocytosis of megalin/cubilin ligands in human PT cells.[22] This was true both for constitutive endocytosis under static conditions and for the higher capacity pathway that is stimulated by acute exposure to fluid shear stress. However, HK-2 cells are a poor model for PT apical endocytosis, and OCRL may modulate endocytic efficiency in more highly differentiated cells. Studies in transgenic zebrafish and in the *Ocrl/Inpp5b* KO/replacement mouse models report defects in PT endocytic uptake.[8,20,21] Reduced endocytosis may reflect a defect in the uncoating of actin-coated endocytic structures as has been suggested[4,5] and/or could be secondary to the lower levels of PT megalin expression noted in both the mouse and zebrafish models.[8,21,20] Reduced levels of shed megalin have also been reported in urine from patients with LS.[38]

An attractive feature of our model is that decreased PT length and/or diameter can also account for the other renal hallmarks of LS, including RTA, hypercalciuria, and aminoaciduria (Figure 6). RTA is thought to be due to reduced Na^+/H^+ exchange *via* NHE3 in the PT and can lead to impaired amino acid transport. A mathematic model for acid reabsorption in the kidney suggests that shorter proximal convoluted tubules would also result in decreased urinary acid excretion.[31] Similarly, Ca^{2+} is thought to be reabsorbed passively along the PT *via* the paracellular pathway[51]; thus, decreased PT length would be expected to result in increased levels of Ca^{2+} reaching distal tubule segments. By contrast, clinical and mathematic modeling studies reveal an excess capacity for glucose uptake by the PT.[31,52,53] For example, loss of 90% of SGLT2 is predicted to lead to only a 40% increase in glucose excretion.[52] Thus, it is likely that a significant reduction in PT length could be tolerated without changes to urinary glucose excretion levels. Of note, although their renal phenotype has been frequently described as Fanconi syndrome, many patients with

LS do not exhibit glycosuria. Moreover, urinary excretion of filtered proteins in patients with LS was considerably higher than that measured in patients with Dent disease or autosomal-dominant idiopathic Fanconi syndrome.[40] Such differences in the characteristic tubular dysfunction observed in genetic diseases that manifest with tubular proteinuria likely reflect the effects of their causative mutations on different pathways.

Increasing appreciation that kidney segment lengths can be dynamically remodeled has significant implications for therapeutic approaches to treat LS. A recent publication demonstrates that pharmacologic activation of an atypical phospholipase C rescues the cytokinesis defect in cells from patients with LS.[54] PT length in rats can be reversibly regulated by >20% in response to prolactin and other hormonal triggers that accompany pregnancy, lactation, and diabetes.[55–59] Such changes are not exclusive to the PT: the length of the distal tubule was observed to elongate in mice fed a high-salt diet.[50] Similarly, Welling and colleagues[60] found that expression of constitutively active SPAK leads to a reduction in connecting tubule mass. Hormonal or pharmacologic interventions may thus be beneficial in treating LS early after diagnosis and could also help re-establish PTs after injury to slow the deterioration of kidney function in patients with LS.

ACKNOWLEDGMENTS

We are very grateful to Martin Lowe for generously providing the transgenic *ocrl*$^{-/-}$ zebrafish line (*via* R. Claudio Aguilar) for these studies, and to tissue donors and the National Institutes of Health NeuroBioBank/University of Maryland School of Medicine Brain and Tissue Bank for access to samples of human kidney. We thank Anatália Labilloy for assistance in generating the CRISPR/Cas9 *OCRL* knockout cells, Francisco Carattino for help with quantifying cilia lengths, Allison Marciszyn for scoring blinded human kidney sections, Roy Zent for providing conditionally immortalized mouse RPTC cells, Polly Mattila for cell culture of mouse RPTCs, Lynda Guzik (McGowan Institute Flow Cytometry Core at University of Pittsburgh) and Frances Alencastro for assistance with FACS sorting, and Sheldon Bastacky for help with assessing human tissue pathology. We appreciate the thoughtful suggestions from a dedicated reviewer for improving our mathematic model of urinary protein excretion.

Dr. Gliozzi and Dr. Weisz designed the study. Dr. Gliozzi, Dr. Espiritu, Ms. Shipman, Mr. Rbaibi, Dr. Long, Dr. Roy, and Dr. Baty carried out experiments. Dr. Gliozzi, Dr. Espiritu, Ms. Shipman, Dr. Duncan, Dr. Hukriede, Dr. Baty, and Dr. Weisz analyzed the data. Dr. Gliozzi, Dr. Espiritu, and Dr. Weisz made the figures. Dr. Gliozzi and Dr. Weisz drafted and revised the paper. All authors approved the final version of the manuscript.

DISCLOSURES

None.

FUNDING

This study was supported by grants from the Lowe Syndrome Association; by National Institutes of Health (NIH) R01 DK101484, R01 DK118726, and S10 OD021627 to Dr. Weisz; NIH R01 DK069403 to Dr. Hukriede; and by the Pittsburgh Center for Kidney Research (P30 DK079307). Dr. Gliozzi was supported by NIH grants T32 DK061296 and TL1 TR001858. Dr. Espiritu was supported by NIH grant T32 DK061296. Ms. Shipman was supported by an American Society of Nephrology predoctoral fellowship award and by NIH F31 DK121394. Dr. Duncan was supported by NIH R01 DK103645.

SUPPLEMENTAL MATERIAL

This article contains the following supplemental material online at http://jasn.asnjournals.org/lookup/suppl/doi:10.1681/ASN.2019020125/-/DCSupplemental.

Supplemental Table 1. Oligonucleotides and primers used in this study.

Supplemental Table 2. Potential off-targets of CRISPR/Cas9 *OCRL* guide sequence.

Supplemental Figure 1. CRISPR/Cas9 *OCRL* clones have no OCRL expression.

Supplemental Figure 2. OCRL depletion slows proliferation of HK-2 cells without increasing apoptosis.

Supplemental Figure 3. *OCRL* knockdown increases multinucleation in mRPTC and hRPTC cell lines.

Supplemental Figure 4. Effect of reduced V_{max} on PT uptake of albumin and LMWP.

Supplemental Figure 5. *Ocrl* morphant zebrafish injected with *ocrl* morpholino have shorter pronephric kidney segments.

Supplemental Figure 5. *Ocrl* morphant zebrafish injected with *ocrl* morpholino have shorter pronephric kidney segments.

Supplemental Figure 6. Acute or chronic depletion of OCRL does not impair endocytic uptake in HK-2 cells.

Supplemental Figure 7. Cilia length in siRNA treated and CRISPR/Cas9 *OCRL* knockout clones.

Supplemental Video 1. Cell division in CRISPR/Cas9 control clone 1.

Supplemental Video 2. Cell division in CRISPR/Cas9 KO clone 2 that resolves into two cells.

Supplemental Video 3. Cell division in CRISPR/Cas9 KO clone 2 that resolves into one multinucleated cell.

REFERENCES

1. Loi M: Lowe syndrome. *Orphanet J Rare Dis* 1: 16, 2006
2. Bockenhauer D, Bokenkamp A, van't Hoff W, Levtchenko E, Kist-van Holthe JE, Tasic V, et al.: Renal phenotype in Lowe Syndrome: A selective proximal tubular dysfunction. *Clin J Am Soc Nephrol* 3: 1430–1436, 2008
3. Mehta ZB, Pietka G, Lowe M: The cellular and physiological functions of the Lowe syndrome protein OCRL1. *Traffic* 15: 471–487, 2014
4. Vicinanza M, Di Campli A, Polishchuk E, Santoro M, Di Tullio G, Godi A, et al.: OCRL controls trafficking through early endosomes via PtdIns4,5P_2-dependent regulation of endosomal actin. *EMBO J* 30: 4970–4985, 2011

5. Nández R, Balkin DM, Messa M, Liang L, Paradise S, Czapla H, et al.: A role of OCRL in clathrin-coated pit dynamics and uncoating revealed by studies of Lowe syndrome cells. *eLife* 3: e02975, 2014
6. Rbaibi Y, Cui S, Mo D, Carattino M, Rohatgi R, Satlin LM, et al.: OCRL1 modulates cilia length in renal epithelial cells. *Traffic* 13: 1295–1305, 2012
7. Coon BG, Hernandez V, Madhivanan K, Mukherjee D, Hanna CB, Barinaga-Rementeria Ramirez I, et al.: The Lowe syndrome protein OCRL1 is involved in primary cilia assembly. *Hum Mol Genet* 21: 1835–1847, 2012
8. Oltrabella F, Pietka G, Ramirez IB, Mironov A, Starborg T, Drummond IA, et al.: The Lowe syndrome protein OCRL1 is required for endocytosis in the zebrafish pronephric tubule. *PLoS Genet* 11: e1005058, 2015
9. Grieve AG, Daniels RD, Sanchez-Heras E, Hayes MJ, Moss SE, Matter K, et al.: Lowe Syndrome protein OCRL1 supports maturation of polarized epithelial cells. *PLoS One* 6: e24044, 2011
10. De Leo MG, Staiano L, Vicinanza M, Luciani A, Carissimo A, Mutarelli M, et al.: Autophagosome-lysosome fusion triggers a lysosomal response mediated by TLR9 and controlled by OCRL. *Nat Cell Biol* 18: 839–850, 2016
11. Dambournet D, Machicoane M, Chesneau L, Sachse M, Rocancourt M, El Marjou A, et al.: Rab35 GTPase and OCRL phosphatase remodel lipids and F-actin for successful cytokinesis. *Nat Cell Biol* 13: 981–988, 2011
12. Ramirez IB, Pietka G, Jones DR, Divecha N, Alia A, Baraban SC, et al.: Impaired neural development in a zebrafish model for Lowe syndrome. *Hum Mol Genet* 21: 1744–1759, 2012
13. Luo N, Kumar A, Conwell M, Weinreb RN, Anderson R, Sun Y: Compensatory role of inositol 5-phosphatase INPP5B to OCRL in primary cilia formation in oculocerebrorenal syndrome of lowe. *PLoS One* 8: e66727, 2013
14. Coon BG, Mukherjee D, Hanna CB, Riese DJ 2nd, Lowe M, Aguilar RC: Lowe syndrome patient fibroblasts display Ocrl1-specific cell migration defects that cannot be rescued by the homologous Inpp5b phosphatase. *Hum Mol Genet* 18: 4478–4491, 2009
15. Montjean R, Aoidi R, Desbois P, Rucci J, Trichet M, Salomon R, et al.: OCRL-mutated fibroblasts from patients with Dent-2 disease exhibit INPP5B-independent phenotypic variability relatively to Lowe syndrome cells. *Hum Mol Genet* 24: 994–1006, 2015
16. Bothwell SP, Farber LW, Hoagland A, Nussbaum RL: Species-specific difference in expression and splice-site choice in Inpp5b, an inositol polyphosphate 5-phosphatase paralogous to the enzyme deficient in Lowe Syndrome. *Mamm Genome* 21: 458–466, 2010
17. Jänne PA, Suchy SF, Bernard D, MacDonald M, Crawley J, Grinberg A, et al.: Functional overlap between murine Inpp5b and Ocrl1 may explain why deficiency of the murine ortholog for OCRL1 does not cause Lowe syndrome in mice. *J Clin Invest* 101: 2042–2053, 1998
18. Bernard DJ, Nussbaum RL: X-inactivation analysis of embryonic lethality in Ocrl wt/-; Inpp5b-/- mice. *Mamm Genome* 21: 186–194, 2010
19. Bothwell SP, Chan E, Bernardini IM, Kuo YM, Gahl WA, Nussbaum RL: Mouse model for Lowe syndrome/Dent Disease 2 renal tubulopathy. *J Am Soc Nephrol* 22: 443–448, 2011
20. Festa BP, Berquez M, Gassama A, Amrein I, Ismail HM, Samardzija M, et al.: OCRL deficiency impairs endolysosomal function in a humanized mouse model for lowe syndrome and dent disease. *Hum Mol Genet* 28: 1931–1946, 2019
21. Inoue K, Balkin DM, Liu L, Nandez R, Wu Y, Tian X, et al.: Kidney tubular ablation of *Ocrl/Inpp5b* phenocopies lowe syndrome tubulopathy. *J Am Soc Nephrol* 28: 1399–1407, 2017
22. Cui S, Guerriero CJ, Szalinski CM, Kinlough CL, Hughey RP, Weisz OA: OCRL1 function in renal epithelial membrane traffic. *Am J Physiol Renal Physiol* 298: F335–F345, 2010
23. Raghavan V, Rbaibi Y, Pastor-Soler NM, Carattino MD, Weisz OA: Shear stress-dependent regulation of apical endocytosis in renal proximal tubule cells mediated by primary cilia. *Proc Natl Acad Sci U S A* 111: 8506–8511, 2014
24. Long KR, Shipman KE, Rbaibi Y, Menshikova EV, Ritov VB, Eshbach ML, et al.: Proximal tubule apical endocytosis is modulated by fluid shear stress via an mTOR-dependent pathway. *Mol Biol Cell* 28: 2508–2517, 2017
25. Gewin L, Vadivelu S, Neelisetty S, Srichai MB, Paueksakon P, Pozzi A, et al.: Deleting the TGF-β receptor attenuates acute proximal tubule injury. *J Am Soc Nephrol* 23: 2001–2011, 2012
26. Olivos-Glander IM, Jänne PA, Nussbaum RL: The oculocerebrorenal syndrome gene product is a 105-kD protein localized to the Golgi complex. *Am J Hum Genet* 57: 817–823, 1995
27. Pereira EM, Labilloy A, Eshbach ML, Roy A, Subramanya AR, Monte S, et al.: Characterization and phosphoproteomic analysis of a human immortalized podocyte model of Fabry disease generated using CRISPR/Cas9 technology. *Am J Physiol Renal Physiol* 311: F1015–F1024, 2016
28. Montague TG, Cruz JM, Gagnon JA, Church GM, Valen E: CHOPCHOP: A CRISPR/Cas9 and TALEN web tool for genome editing. *Nucleic Acids Res* 42: W401-7, 2014
29. Duncan AW, Taylor MH, Hickey RD, Hanlon Newell AE, Lenzi ML, Olson SB, et al.: The ploidy conveyor of mature hepatocytes as a source of genetic variation. *Nature* 467: 707–710, 2010
30. Lazzara MJ, Deen WM: Model of albumin reabsorption in the proximal tubule. *Am J Physiol Renal Physiol* 292: F430–F439, 2007
31. Weinstein AM, Weinbaum S, Duan Y, Du Z, Yan Q, Wang T: Flow-dependent transport in a mathematical model of rat proximal tubule. *Am J Physiol Renal Physiol* 292: F1164–F1181, 2007
32. Kelman RB: A theoretical note on exponential flow in the proximal part of the mammalian nephron. *Bull Math Biophys* 24: 303–317, 1962
33. Layton AT, Layton HE: A computational model of epithelial solute and water transport along a human nephron. *PLOS Comput Biol* 15: e1006108, 2019
34. Savory DJ: Reference ranges for serum creatinine in infants, children and adolescents. *Ann Clin Biochem* 27: 99–101, 1990
35. Park CH, Maack T: Albumin absorption and catabolism by isolated perfused proximal convoluted tubules of the rabbit. *J Clin Invest* 73: 767–777, 1984
36. Tojo A, Endou H: Intrarenal handling of proteins in rats using fractional micropuncture technique. *Am J Physiol* 263: F601–F606, 1992
37. Koeppen BM, Stanton BA: *Renal Physiology*, Philadelphia, Mosby Elsevier, 2007
38. Norden AG, Lapsley M, Igarashi T, Kelleher CL, Lee PJ, Matsuyama T, et al.: Urinary megalin deficiency implicates abnormal tubular endocytic function in Fanconi syndrome. *J Am Soc Nephrol* 13: 125–133, 2002
39. Bernard A, Viau C, Ouled A, Lauwerys R: Competition between low- and high-molecular-weight proteins for renal tubular uptake. *Nephron* 45: 115–118, 1987
40. Norden AG, Lapsley M, Lee PJ, Pusey CD, Scheinman SJ, Tam FW, et al.: Glomerular protein sieving and implications for renal failure in Fanconi syndrome. *Kidney Int* 60: 1885–1892, 2001
41. Kimmel CB, Ballard WW, Kimmel SR, Ullmann B, Schilling TF: Stages of embryonic development of the zebrafish. *Dev Dyn* 203: 253–310, 1995
42. de Groh ED, Swanhart LM, Cosentino CC, Jackson RL, Dai W, Kitchens CA, et al.: Inhibition of histone deacetylase expands the renal progenitor cell population. *J Am Soc Nephrol* 21: 794–802, 2010
43. Neugarten J, Aynedjian HS, Bank N: Role of tubular obstruction in acute renal failure due to gentamicin. *Kidney Int* 24: 330–335, 1983
44. Kur E, Christa A, Veth KN, Gajera CR, Andrade-Navarro MA, Zhang J, et al.: Loss of Lrp2 in zebrafish disrupts pronephric tubular clearance but not forebrain development. *Dev Dyn* 240: 1567–1577, 2011
45. Wingert RA, Selleck R, Yu J, Song HD, Chen Z, Song A, et al.: The cdx genes and retinoic acid control the positioning and segmentation of the zebrafish pronephros. *PLoS Genet* 3: 1922–1938, 2007
46. Horsfield J, Ramachandran A, Reuter K, LaVallie E, Collins-Racie L, Crosier K, et al.: Cadherin-17 is required to maintain pronephric duct integrity during zebrafish development. *Mech Dev* 115: 15–26, 2002
47. Madhivanan K, Ramadesikan S, Aguilar RC: Role of Ocrl1 in primary cilia assembly. *Int Rev Cell Mol Biol* 317: 331–347, 2015

48. Hsieh WC, Ramadesikan S, Fekete D, Aguilar RC: Kidney-differentiated cells derived from Lowe Syndrome patient's iPSCs show ciliogenesis defects and Six2 retention at the Golgi complex. *PLoS One* 13: e0192635, 2018
49. Fetterman GH, Shuplock NA, Philipp FJ, Gregg HS: The growth and maturation of human glomeruli and proximal convolutions from term to adulthood: Studies by microdissection. *Pediatrics* 35: 601–619, 1965
50. Walton SL, Moritz KM, Bertram JF, Singh RR: Lengths of nephron tubule segments and collecting ducts in the CD-1 mouse kidney: An ontogeny study. *Am J Physiol Renal Physiol* 311: F976–F983, 2016
51. Moor MB, Bonny O: Ways of calcium reabsorption in the kidney. *Am J Physiol Renal Physiol* 310: F1337–F1350, 2016
52. Weinstein AM: A mathematical model of the rat nephron: Glucose transport. *Am J Physiol Renal Physiol* 308: F1098–F1118, 2015
53. Govaerts P: Physiopathology of glucose excretion by the human kidney. *BMJ* 2: 175–179, 1952
54. Mondin VE, Ben El Kadhi K, Cauvin C, Jackson-Crawford A, Bélanger E, Decelle B, et al.: PTEN reduces endosomal PtdIns(4,5)P_2 in a phosphatase-independent manner via a PLC pathway. *J Cell Biol* 218: 2198–2214, 2019
55. Garland HO, Green R, Moriarty RJ: Changes in body weight, kidney weight and proximal tubule length during pregnancy in the rat. *Ren Physiol* 1: 42–47, 1978
56. Arthur SK, Green R: Fluid reabsorption by the proximal convoluted tubule of the kidney in lactating rats. *J Physiol* 371: 267–275, 1986
57. Elkarib AO, Garland HO, Green R: Acute and chronic effects of progesterone and prolactin on renal function in the rat. *J Physiol* 337: 389–400, 1983
58. Rasch R, Dørup J: Quantitative morphology of the rat kidney during diabetes mellitus and insulin treatment. *Diabetologia* 40: 802–809, 1997
59. Seyer-Hansen K, Hansen J, Gundersen HJ: Renal hypertrophy in experimental diabetes. A morphometric study. *Diabetologia* 18: 501–505, 1980
60. Grimm PR, Coleman R, Delpire E, Welling PA: Constitutively active SPAK causes hyperkalemia by activating NCC and remodeling distal tubules. *J Am Soc Nephrol* 28: 2597–2606, 2017